photonics

MDPI

Article

Polarization Characteristics of AlO Molecular Spectra in Femtosecond Laser-Induced Aluminum Plasma

Xuefeng Chu [1], Qiuyun Wang [1] and Xun Gao [1,2,*]

[1] School of Physics, Changchun University of Science and Technology, Changchun 130022, China; chuxuefeng@mails.cust.edu.cn (X.C.); wangqiuyun@cust.edu.cn (Q.W.)
[2] Zhongshan Institute, Changchun University of Science and Technology, Zhongshan 528437, China
* Correspondence: gaoxun@cust.edu.cn

Abstract

To investigate the polarization characteristics of AlO molecular emission in femtosecond laser-induced aluminum plasma, AlO molecular spectra were generated by irradiating an aluminum target with a femtosecond laser. The experimental results revealed a pronounced polarization response in the AlO emission. After a polarizer was introduced into the collection path, the signal-to-background ratio (SBR) increased from 8.30 to 10.80, while the relative standard deviation (RSD) decreased from 0.043 to 0.036, indicating improved spectral quality and stability. By modulating the laser polarization state using a half-wave plate and a quarter-wave plate, the AlO spectral intensity increased by a factor of 1.26 when the laser polarization was changed from horizontal to vertical, and by a factor of 1.75 when it was changed from linear to circular. Under circular, horizontal, and vertical polarization conditions, the SBR values obtained with a polarizer were consistently higher than those obtained without a polarizer, with the maximum value of 12.46 achieved under vertical polarization. These results demonstrate that both plasma polarization detection and laser polarization modulation can effectively achieve better-quality AlO molecular spectra. This work provides a useful reference for improving molecular spectral quality in femtosecond laser-induced spectroscopy.

Keywords: femtosecond laser; AlO molecular spectra; polarization; SBR; RSD; spectral quality

1. Introduction

As a powerful analytical technique, laser-based spectroscopy has attracted considerable attention in material characterization and compositional analysis owing to its high accuracy, rapid response, non or minimum sample preparation and non-invasive nature [1–3]. A variety of techniques, including absorption spectroscopy [4–6], photoacoustic spectroscopy [7–9], and photothermal spectroscopy [10–13], have been continuously developed, thereby greatly expanding the application scope of spectroscopic detection. Among these methods, laser-induced plasma optical emission spectroscopy, which is characterized by its capability for in situ, real-time, and simultaneous multi-element analysis, has become an important tool for plasma diagnostics and material analysis [14–20]. In most Laser-Induced Breakdown Spectroscopy (LIBS) studies, atomic and ionic emission lines are typically used as the primary analytical signals due to their relatively high emission intensity and well-established quantitative calibration methods. However, during plasma

Check for updates

Received: 9 April 2026
Revised: 13 May 2026
Accepted: 19 May 2026
Published: 20 May 2026

Copyright: © 2026 by the authors. Licensee MDPI, Basel, Switzerland. This article is an open access article distributed under the terms and conditions of the Creative Commons Attribution (CC BY) license.

expansion in ambient air, stable molecular species can also be formed [21,22]. The emission bands of these molecules provide valuable chemical information, including isotopic ratios [23,24], halogen content [25], and the presence of explosive residues [26]. Accordingly, molecular emission in LIBS has attracted increasing attention as a useful source of complementary analytical information. Recent studies and reviews have highlighted the growing importance of molecular bands in LIBS for improving analytical specificity and extending LIBS analysis to the molecular domain [27–32]. Related numerical studies have suggested that thermochemical non-equilibrium may affect molecular emission during plasma expansion [33–35].

AlO is a highly useful molecular emitter in laser-induced plasmas. Its simple diatomic structure and well-defined electronic transitions make it an effective probe for investigating plasma-plume evolution, reaction pathways, and energy-transfer dynamics [36,37]. Earlier work has explored the temporal and spatial behavior of AlO under both femtosecond and nanosecond laser ablation. Harilal et al. [38] reported that AlO appeared at the earliest stage under femtosecond irradiation, whereas its emission persisted for the longest time under nanosecond conditions. Guo et al. [39] showed that AlO emission emerges later than Al atomic lines, which was attributed to delayed molecular formation during plasma cooling.

Although laser-induced breakdown spectroscopy has found use in a range of practical applications, further improvement in signal-to-background contrast, spectral stability, and quantitative reliability is still desirable for more robust analytical performance [40–43]. For this reason, many studies have focused on methods capable of increasing spectral intensity and achieving more reproducible measurements, including plasma modulation [44], double-pulse excitation [45], surface-enhanced techniques [46,47], time-resolved LIBS and spatially resolved LIBS [48,49]. Among these approaches, polarization-resolved LIBS (PR-LIBS) has emerged as a simple and cost-effective method for improving the SBR and spectral reproducibility. Penczak et al. [50] demonstrated that PR-LIBS can effectively suppress the continuum background by distinguishing between different polarization components of plasma emission, thereby enhancing the SBR and improving measurement stability. Zhao et al. [51] further combined PR-LIBS with partial least squares (PLS) regression to develop a hybrid model for steel alloy analysis, achieving improved analytical performance, with the coefficient of determination (R^2) showing an improvement of at least 3.4%, whereas the root mean square error of calibration (RMSEC) and prediction (RMSEP) decreasing by 6.3% and 19.0%, respectively. Through a comparison of Cu and Al atomic-emission ratios under polarizer and non-polarizer conditions, Eslami et al. [52] reported that use of a polarizer leads to a significant improvement in the SBR of atomic spectra. Most of the available studies, however, have centered predominantly on emissions from atoms and ions, while investigations into the polarization characteristics of molecular species remain limited. As a result, the application potential of polarization-based approaches in improving molecular spectral quality remains constrained.

In this work, polarization-based techniques are systematically explored as a means of improving the quality of AlO molecular emission in femtosecond-laser-generated aluminum plasma. First, the role of plasma polarization in improving spectral quality is evaluated. Then, the effect of the laser polarization state on AlO emission intensity is analyzed. Finally, the potential for further improving spectral quality under different laser polarization conditions is assessed.

2. Materials and Methods

Figure 1 illustrates the experimental arrangement employed for analysis of the polarization properties of AlO molecular spectra. Plasma generation was achieved using a

femtosecond laser system (Libra, Coherent Inc., Santa Clara, CA, USA). The laser delivered pulses at 800 nm with a duration of 50 fs, operated at a repetition rate of 1.0 kHz, and showed an energy stability of 0.5%. Throughout the measurements, the pulse energy was kept constant at 1.8 mJ. The laser beam was focused onto the surface of an aluminum target using a plano-convex quartz lens (L1, with a focal length of 100 mm) to generate plasma. The pulse energy was adjusted using an attenuator consisting of a half-wave plate and a Glan polarizer. The incident laser polarization was tuned through rotation of a half-wave plate or a quarter-wave plate installed ahead of L1, without altering the laser pulse energy. A fused-silica lens (L2, 75 mm focal length) was used to collect the emitted plasma light, which was subsequently guided by an eight-channel fiber bundle (FC8-UVIR200-2) into an eight-channel spectrometer (AvaSpec-2048, Avantes B.V., Apeldoorn, The Netherlands; spectral range: 200–1100 nm) for spectral measurement. To minimize interference from the strong early-time continuum emission, spectral acquisition was performed with a delay of 2 μs and an integration time of 1.05 ms. Under these conditions, the AlO molecular emission showed relatively strong intensity with clear and well-defined spectral features. The laser trigger and spectral acquisition were temporally synchronized by means of a digital delay generator (DG645, Stanford Research Systems Inc., Sunnyvale, CA, USA). To ensure that successive laser pulses irradiated fresh areas of the surface, the target was continuously shifted along the *Y*-axis at a constant speed by means of a three-dimensional translation stage. A linear polarizer (operating over 400–700 nm) was placed between L2 and the fiber probe. Rotation of the analyzer made it possible to record AlO molecular spectra under different polarization-angle conditions for later polarization analysis. To improve signal stability and reduce experimental uncertainty, we have also clarified the data-processing procedure. Each reported spectral value was calculated from the average of 8 independently recorded spectra acquired under the same experimental conditions, and each individual spectrum was obtained by averaging the signals from 30 laser shots. In addition, the software used for spectral processing has now been specified as Origin. The material used in this work was a 1060-grade aluminum plate supplied by Shenzhen Lütai Industrial Co., Ltd., Shenzhen, China, with an Al content of 99.61%. All experiments were conducted under ambient conditions at a temperature of 22 °C and a relative humidity of 28%.

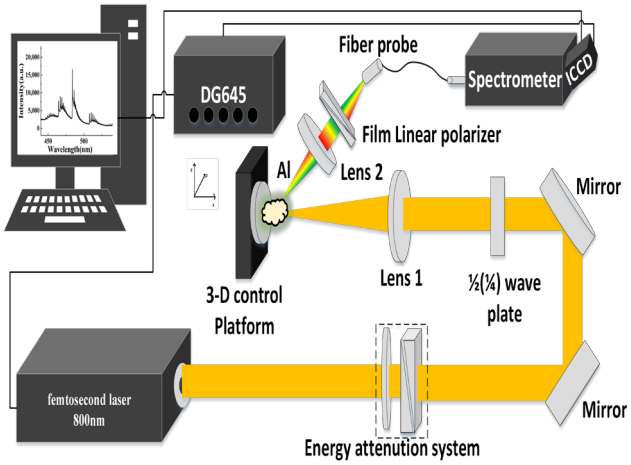

Figure 1. Schematic illustration of the experimental arrangement.

3. Results and Discussion

3.1. Influence of Plasma Polarization on AlO Molecular Spectral Quality

The polarization characteristics of the AlO molecular spectra were investigated by introducing a thin-film linear polarizer into the collection path upstream of the spectrometer

fiber. This experimental design permitted a direct assessment of the polarization behavior of the emitted plasma radiation. Spectra were first recorded with and without the polarizer, as shown in Figure 2.

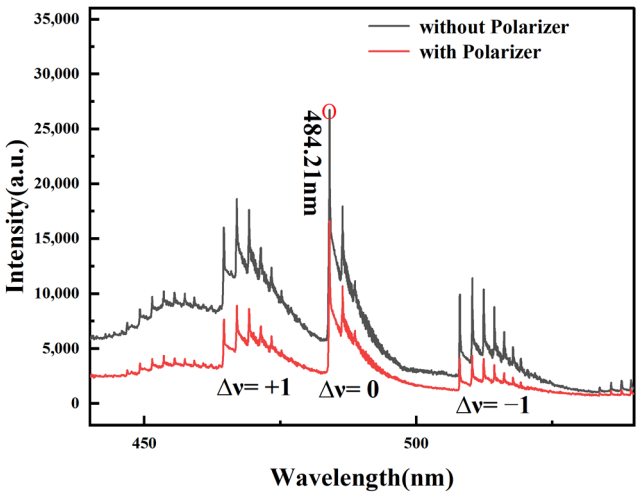

Figure 2. The AlO emission spectra with and without a polarizer. The red circle marks the 484.21 nm spectral line.

Figure 2 shows the AlO emission spectra recorded with and without a polarizer. The main molecular features in this spectral region are assigned to the AlO $B^2\Sigma^+$–$X^2\Sigma^+$ system, including the $\Delta v = +1$, $\Delta v = 0$, and $\Delta v = -1$ vibrational bands. Among them, the band near 484.21 nm, corresponding to the $\Delta v = 0$ transition, was selected as the representative peak for the subsequent polarization analysis, because it is one of the most distinct and intense molecular features in the measured spectrum. As can be seen, after the polarizer was introduced, the overall spectral intensity decreased, while the main AlO molecular features remained identifiable. These observations suggest that the polarizer affects both the total collected emission and the spectral background. The corresponding improvement in spectral quality is further evaluated quantitatively in the following analysis.

To gain further insight into the role of polarizer angle in determining molecular emission intensity, the polarizer was rotated from 0° to 360° in steps of 20°, and spectra were recorded at each angular position to fully characterize the variation in polarized intensity. Figure 3 illustrates how the peak intensity of the 484.21 nm AlO molecular emission line changes with polarizer angle. This line corresponds to the $B^2\Sigma^+$–$X^2\Sigma^+$ electronic transition with a vibrational quantum number difference of $\Delta v = 0$. The observed angular dependence reveals the influence of polarization on both the continuum emission and the molecular spectral signal. Fitting the experimental data showed that the peak intensities of the AlO molecular emission follow Malus's law:

$$I = I_0 \cos^2 \theta \quad (1)$$

where θ is defined as the angle between the polarization direction of the incident light and the transmission axis of the analyzer. The observed angular dependence indicates that the AlO emission exhibit clear linear polarization. As a heteronuclear diatomic molecule, AlO possesses a non-zero transition dipole moment arising from the difference in electronegativity between aluminum and oxygen, leading to a non-uniform charge distribution. During radiative transitions between the excited and ground states, this dipole moment renders the emission direction-dependent, and the corresponding AlO spectral lines may therefore exhibit polarization [53].

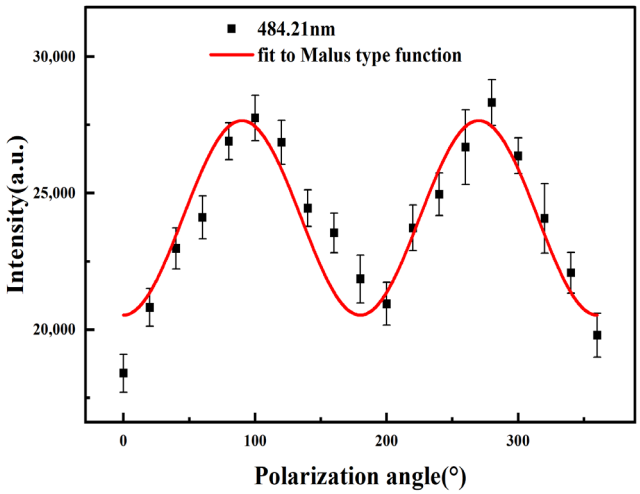

Figure 3. Variation in the AlO peak intensity at 484.21 nm with the polarizer angle.

In addition, AlO molecules are mainly formed near the plasma–air interface, where strong temperature gradients and flow effects can induce preferential molecular orientation. It should also be noted that the formation and emission of AlO molecules may be influenced by thermochemical non-equilibrium during plume expansion. Near the plasma–air interface, species diffusion and non-equilibrium chemical reactions may affect the local population of AlO and its radiative behavior [33]. This preferred alignment further contributes to the partial polarization of AlO molecular emission. Unlike continuum radiation, which is mainly associated with isotropic free-electron processes, the formation and radiative emission of AlO molecules are intrinsically anisotropic, resulting in more pronounced polarization behavior [54]. A quantitative treatment of the non-equilibrium effects would require dedicated numerical modeling and is beyond the scope of the present work.

To explore more deeply the role of plasma polarization in shaping AlO spectral quality, the characteristic peak at 484.21 nm was selected, and the variations in peak intensity with the number of spectral acquisitions, together with the corresponding SBR and RSD values, were compared with and without a polarizer. As shown in Figure 4a, without the polarizer, the peak intensity of AlO at 484.21 nm was generally higher, but the fluctuations were more pronounced, resulting in an RSD of 4.3%. After the polarizer was introduced, the overall peak intensity decreased, whereas the signal fluctuations became smaller and more stable, and the RSD was reduced to 3.6%. This indicates that although the polarizer attenuated part of the total emission intensity, it effectively suppressed signal fluctuations and improved measurement repeatability.

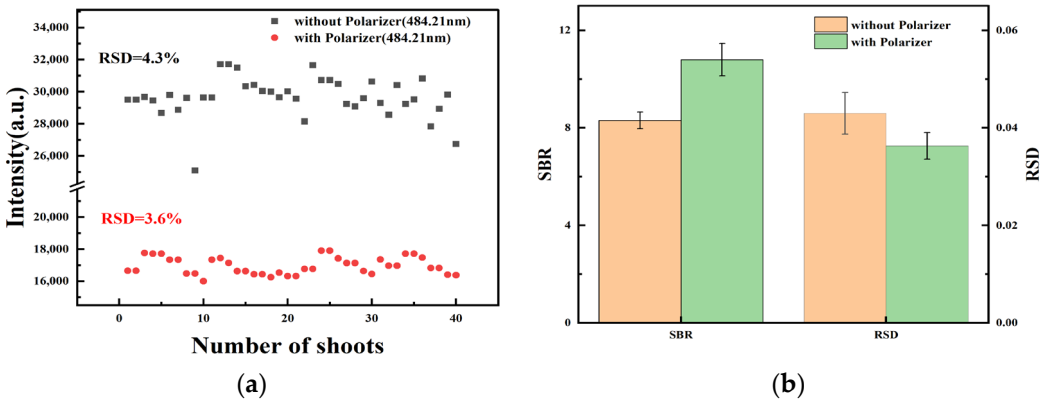

Figure 4. (**a**) Variation in the peak intensity of AlO (484.21 nm) with the number of laser shots; (**b**) SBR and RSD of AlO (484.21 nm) with and without polarization.

As shown in Figure 4b, after the polarizer was introduced, the SBR of AlO at 484.21 nm increased from 8.3 to 10.8, representing an improvement of approximately 30.1%, while the RSD decreased from 4.3% to 3.6%, corresponding to a reduction of approximately 16.3%. These results demonstrate that plasma polarization can serve as an effective means of spectral optimization, thereby improving both the quality and repeatability of AlO molecular spectra.

3.2. Influence of Laser Polarization on the AlO Molecular Spectrum

In the previous experiments, the incident laser was set to be horizontally polarized. To examine how laser polarization affects AlO molecular emission, the optical path was equipped with either a half-wave plate or a quarter-wave plate. As shown in Figure 5 when the linear laser polarization was changed from horizontal to vertical by rotating the half-wave plate, the AlO spectral intensity increased continuously, and the intensity under vertical polarization was 1.26 times higher than that under horizontal polarization. This result indicates that AlO emission is strongly dependent on the laser polarization direction. This behavior is associated with the intrinsic anisotropy of AlO molecules, whose transition dipole moment is aligned along the molecular axis, rendering the excitation efficiency sensitive to the direction of the laser electric field. More efficient coupling under vertical polarization enhances the $B^2\Sigma^+$–$X^2\Sigma^+$ electronic transition. In addition, polarization-dependent electron motion may alter the collisional processes at the plasma-air interface and promote AlO formation, thereby further strengthening the molecular emission [50,55].

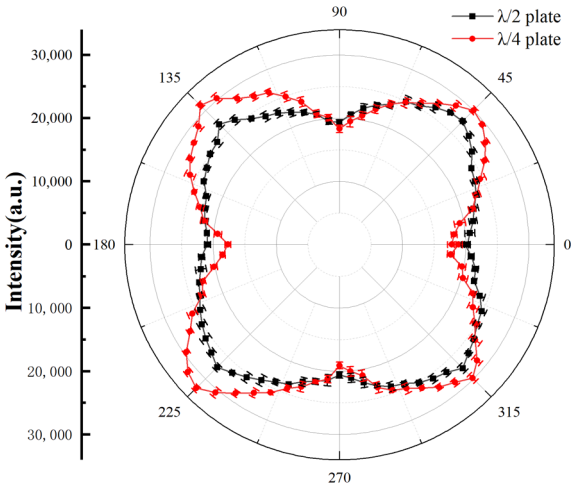

Figure 5. Variation in the AlO spectral intensity with the half-wave plate rotation angle and the quarter-wave plate rotation angle.

As also shown in Figure 5 when the quarter-wave plate was rotated to convert the laser polarization from linear to circular, the AlO spectral intensity also increased continuously. The intensity under circular polarization was 1.75-fold that under linear polarization, suggesting that the ellipticity of the laser polarization also has a pronounced effect on AlO emission. Previous studies have reported stronger AlO molecular band emission under circular polarization in femtosecond LIBS. This improvement is usually attributed to the fact that circular polarization produces free electrons with higher kinetic energy, which affect the plasma temperature, density, and evolution, and consequently influence the formation and radiative emission of AlO molecules [56]. Overall, these results demonstrate that the laser polarization state plays a key role in determining the intensity of AlO molecular emission.

To examine more thoroughly the role of laser polarization in shaping the polarization characteristics of plasma emission, the SBR and RSD of the AlO molecular spectra were compared with and without a polarizer in the collection path under circular, horizontal, and vertical laser polarization conditions. The polarizer angle was fixed at 90°.

As shown in Figure 6a, the SBR values obtained with the polarizer were markedly higher than those obtained without it under all three laser polarization conditions, indicating that polarization filtering can effectively improve the SBR of the AlO spectra. Besides, under both detection conditions, the highest SBR was obtained with vertical laser polarization, followed by circular polarization, whereas horizontal polarization yielded the lowest SBR. This result suggests that the laser polarization state has a clear influence on spectral quality and that vertical polarization is more favorable for achieving a higher SBR. As shown in Figure 6b, the RSD values under all three laser polarization conditions decreased after the polarizer was introduced, indicating that polarization filtering also improves measurement stability. By contrast, the differences in RSD among the three laser polarization states were relatively small, suggesting that laser polarization has no significant effect on spectral repeatability. The results show that molecular-emission polarization characteristics are strongly dependent on the laser polarization state, and that the highest-quality AlO spectra are obtained under vertical polarization. These findings suggest that integrating the plasma polarization with modulation of the laser polarization state may provide an effective route to further improve the quality of femtosecond-laser-induced AlO molecular spectra.

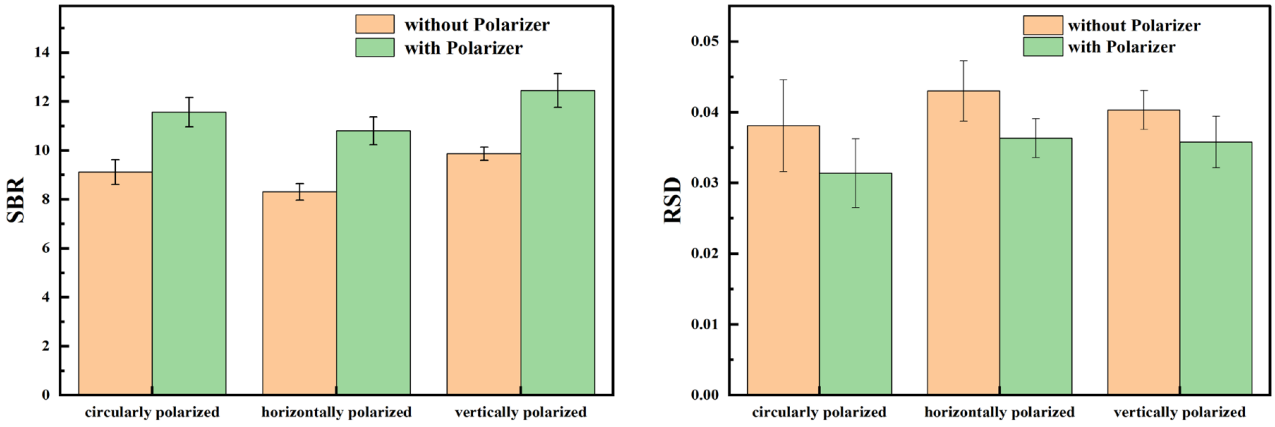

(**a**) (**b**)

Figure 6. (**a**) SBR and (**b**) RSD of the AlO spectrum with and without a polarizer under horizontal, circular, and vertical laser polarization conditions.

4. Conclusions

AlO molecular emission from femtosecond-laser-produced aluminum plasma was systematically analyzed with respect to its polarization characteristics. The measurements revealed a clear polarization of the AlO emission. When a polarizer was inserted into the collection path, the signal-to-background ratio increased and the relative standard deviation of the AlO spectra decreased, demonstrating that polarization-based collection can improve both spectral quality and measurement stability. By adjusting the laser polarization state through a half-wave plate together with a quarter-wave plate, it was further demonstrated that the AlO spectral intensity increased when the laser polarization was changed from horizontal to vertical and from linear to circular. It is found that by combining plasma polarization with laser polarization state modulation, the SBR of the AlO

spectra was strongly dependent on the laser polarization state, with vertical polarization providing the highest SBR and thus the best spectral quality. By contrast, the RSD showed only minor variation under different laser polarization conditions, suggesting that laser polarization has little effect on spectral repeatability. Overall, these results demonstrate that polarization-based methods provide a simple and effective strategy for improving the quality of molecular spectra in femtosecond laser-induced plasma.

Author Contributions: X.C.: Data curation, Writing-original draft preparation, Investigation; Q.W.: Supervision, Formal analysis; X.G.: Project administration, Writing-review and editing, Funding acquisition. All authors have read and agreed to the published version of the manuscript.

Funding: This research was supported by the National Natural Science Foundation of China (Grant No. 62575035) and the Natural Science Foundation of Jilin Province (Grant No. 20260102235JC).

Data Availability Statement: The raw data supporting the conclusions of this article will be made available by the authors on request.

Conflicts of Interest: The authors declare no conflicts of interest.

References

1. Liu, Z.; Ni, J.; Tang, Z.; Wang, Q.J.; Yu, X. Advanced Mid-Infrared Laser Spectroscopy for Ultra-Low Concentration Protein Detection. *Laser Photonics Rev.* **2025**, *19*, e00718. [CrossRef]
2. Sun, H.; Qiao, S.; He, Y.; Sun, X.; Ma, Y. Parts-per-quadrillion level gas molecule detection: CO-LITES sensing. *Light Sci. Appl.* **2025**, *14*, 180. [CrossRef]
3. Yufei, M.; Yahui, L.; Ying, H.; Shunda, Q.; Haiyue, S. Design of multipass cell with dense spot patterns and its performance in a light-induced thermoelastic spectroscopy-based methane sensor. *Light Adv. Manuf.* **2025**, *6*, 5–13. [CrossRef]
4. Shi, Y.; Huang, D.; Li, F.; Zheng, K.; Li, Q.; Jin, W. High-sensitivity, real-time, multi-gas sensing based on a 100 MHz-rate time-stretch wavelength swept laser absorption spectroscopy. *Opt. Laser Technol.* **2026**, *199*, 115059. [CrossRef]
5. Xu, L.; Cai, Q.; Xu, D.; Wu, H.; Zhang, G.; Ge, Q.; Li, J. Calibration-free quartz tuning fork enhanced laser spectroscopy for trace gas detection. *Sens. Actuators B Chem.* **2026**, *447*, 138854. [CrossRef]
6. Wang, R.; Han, G.; He, Y.; Qiao, S.; Ma, Y. Lithium niobate tuning fork-enhanced photoacoustic spectroscopy and light-induced thermoelastic spectroscopy. *Appl. Phys. Rev.* **2025**, *12*, 041404. [CrossRef]
7. Cheng, H.; Zeng, F.; Chao, X.; Jiang, X.; Fang, Z. Signal correction using transmitted spot information: A low error photoacoustic spectroscopy-based gas detection system. *Sens. Actuators A Phys.* **2025**, *383*, 116179. [CrossRef]
8. Wijesinghe, D.R.; Zobair, M.A.; Esmaeelpour, M. A Review on Photoacoustic Spectroscopy Techniques for Gas Sensing. *Sensors* **2024**, *24*, 6577. [CrossRef]
9. Mu, J.; Han, G.; Wang, R.; Qiao, S.; He, Y.; Ma, Y. Photoacoustic spectroscopy and light-induced thermoelastic spectroscopy based on inverted-triangular lithium niobate tuning fork. *Opto-Electron. Sci.* **2025**, *4*, 250035. [CrossRef]
10. Zhu, L.; Wan, F.; Bai, Y.; Sun, H.; Wu, Y.; Chen, W. A review of photothermal spectroscopy for gas sensing. *Microchem. J.* **2026**, *220*, 116716. [CrossRef]
11. Zheng, K.; Pi, M.; Huang, Y.; Peng, Z.; Zhao, H.; Song, F.; Bao, H.; Jiang, S.; Ho, H.L.; Zheng, C.; et al. Waveguide-Based On-Chip Photothermal Spectroscopy for Gas Sensing. *Laser Photonics Rev.* **2024**, *18*, 2301071. [CrossRef]
12. Li, C.; He, Y.; Qiao, S.; Ma, Y. Indirect detection of hydrogen based on light-induced thermoelastic spectroscopy. *Opt. Express* **2026**, *34*, 1905–1918. [CrossRef] [PubMed]
13. Ma, H.; Qiao, S.; He, Y.; Zhang, C.; Ma, Y. Overtone acoustic feedback enhanced light-induced thermoelastic spectroscopy sensing. *Photonics Res.* **2026**, *14*, 683–689. [CrossRef]
14. Wang, Z.; Afgan, M.; Gu, W.; Song, Y.; Wang, Y.; Hou, Z.; Song, W.; Li, Z. Recent advances in laser-induced breakdown spectroscopy quantification: From fundamental understanding to data processing. *TrAC Trends Anal. Chem.* **2021**, *143*, 116385. [CrossRef]
15. Zhao, S.; Song, W.; Hou, Z.; Wang, Z. Classification of ginseng according to plant species, geographical origin, and age using laser-induced breakdown spectroscopy and hyperspectral imaging. *J. Anal. At. Spectrom.* **2021**, *36*, 1704–1711. [CrossRef]
16. Wang, Z.; Dong, F.; Zhou, W. A Rising Force for the World-Wide Development of Laser-Induced Breakdown Spectroscopy. *Plasma Sci. Technol.* **2015**, *17*, 617–620. [CrossRef]
17. Chen, Z.; Li, H.; Liu, M.; Li, R. Fast and sensitive trace metal analysis in aqueous solutions by laser-induced breakdown spectroscopy using wood slice substrates. *Spectrochim. Acta Part B At. Spectrosc.* **2008**, *63*, 64–68. [CrossRef]

18. Yoshino, S.; Thornton, B.; Takahashi, T.; Takaya, Y.; Nozaki, T. Signal preprocessing of deep-sea laser-induced plasma spectra for identification of pelletized hydrothermal deposits using Artificial Neural Networks. *Spectrochim. Acta Part B At. Spectrosc.* **2018**, *145*, 1–7. [CrossRef]
19. Burger, M.; Finney, L.A.; Garrett, L.; Harilal, S.S.; Hartig, K.C.; Nees, J.; Skrodzki, P.J.; Xiao, X.; Jovanovic, I. Laser ablation spectrometry for studies of uranium plasmas, reactor monitoring, and spent fuel safety. *Spectrochim. Acta Part B At. Spectrosc.* **2021**, *179*, 106095. [CrossRef]
20. Courreges-Lacoste, G.B.; Ahlers, B.; Pérez, F.R. Combined Raman spectrometer/laser-induced breakdown spectrometer for the next ESA mission to Mars. *Spectrochim. Acta Part A Mol. Biomol. Spectrosc.* **2007**, *68*, 1023–1028. [CrossRef]
21. De Giacomo, A.; Hermann, J. Laser-induced plasma emission: From atomic to molecular spectra. *J. Phys. D Appl. Phys.* **2017**, *50*, 183002. [CrossRef]
22. Ran, P.; Hou, H.; Luo, S.-N. Molecule formation induced by non-uniform plume-air interactions in laser induced plasma. *J. Anal. At. Spectrom.* **2017**, *32*, 2254–2262. [CrossRef]
23. Dong, M.; Chan, G.C.-Y.; Mao, X.; Gonzalez, J.J.; Lu, J.; Russo, R.E. Elucidation of C2 and CN formation mechanisms in laser-induced plasmas through correlation analysis of carbon isotopic ratio. *Spectrochim. Acta Part B At. Spectrosc.* **2014**, *100*, 62–69. [CrossRef]
24. Bol'shakov, A.A.; Mao, X.; González, J.J.; Russo, R.E. Laser ablation molecular isotopic spectrometry (LAMIS): Current state of the art. *J. Anal. At. Spectrom.* **2016**, *31*, 119–134. [CrossRef]
25. Álvarez, C.; Pisonero, J.; Bordel, N. Quantification of fluorite mass-content in powdered ores using a Laser-Induced Breakdown Spectroscopy method based on the detection of minor elements and CaF molecular bands. *Spectrochim. Acta Part B At. Spectrosc.* **2014**, *100*, 123–128. [CrossRef]
26. Lopez-Moreno, C.; Palanco, S.; Laserna, J.J.; DeLucia, F., Jr.; Miziolek, A.W.; Rose, J.; Walters, R.A.; Whitehouse, A.I. Test of a stand-off laser-induced breakdown spectroscopy sensor for the detection of explosive residues on solid surfaces. *J. Anal. At. Spectrom.* **2006**, *21*, 55–60. [CrossRef]
27. Xu, F.; Ma, S.; Zhao, C.; Dong, D. Application of Molecular Emissions in Laser-Induced Breakdown Spectroscopy: A Review. *Front. Phys.* **2022**, *10*, 821528. [CrossRef]
28. Gaft, M.; Nagli, L.; Gornushkin, I.; Raichlin, Y. Review on recent advances in analytical applications of molecular emission and modelling. *Spectrochim. Acta Part B At. Spectrosc.* **2020**, *173*, 105989. [CrossRef]
29. Fernández-Bravo, Á.; Delgado, T.; Lucena, P.; Laserna, J.J. Vibrational emission analysis of the CN molecules in laser-induced breakdown spectroscopy of organic compounds. *Spectrochim. Acta Part B At. Spectrosc.* **2013**, *89*, 77–83. [CrossRef]
30. Dong, M.; Lu, J.; Yao, S.; Zhong, Z.; Li, J.; Li, J.; Lu, W. Experimental study on the characteristics of molecular emission spectroscopy for the analysis of solid materials containing C and N. *Opt. Express* **2011**, *19*, 17021–17029. [CrossRef]
31. Jia, Z.; Tian, Y.; Li, L.; Xue, C.; Guo, J.; Lu, Y.; Zhang, X.; Zheng, R. Comparison of ionic, atomic and molecular emissions in underwater laser-induced breakdown spectroscopy for quantitative analysis of Ca and Sr. *J. Anal. At. Spectrom.* **2026**, *Advance Article*. [CrossRef]
32. Santos, M.B.D.; Galli, L.L.; Villas-Boas, P.R. Sulfur quantification by LIBS using CS molecular emissions in synthetic and plant-based samples under atmospheric conditions. *Spectrochim. Acta Part B At. Spectrosc.* **2026**, *237*, 107427. [CrossRef]
33. Colonna, G.; Pascazio, G.; Bonelli, F. Advanced model for the interaction of a Ti plume produced by a ns-pulsed laser in a nitrogen environment. *Spectrochim. Acta Part B At. Spectrosc.* **2021**, *179*, 106120. [CrossRef]
34. Chemin, A.; Ross, A.; Hermelin, S.; Crozet, P.; Motto-Ros, V.; Ledoux, G.; Dujardin, C.; Amans, D. On the use of laser-induced fluorescence to probe the thermodynamic equilibrium in laser-generated plasmas. *Spectrochim. Acta Part B At. Spectrosc.* **2023**, *205*, 106685. [CrossRef]
35. Surmick, D.M.; Dagel, D.J.; Parigger, C.G. Spatial Molecular AlO Temperature Distributions in Laser-Induced Plasma. *Atoms* **2019**, *7*, 86. [CrossRef]
36. Yuasa, S.; Zhu, Y.; Sogo, S. Ignition and combustion of aluminum in oxygen/nitrogen mixture streams. *Combust. Flame* **1997**, *108*, 387–396. [CrossRef]
37. Wang, Q.; Chen, A.; Xu, W.; Zhang, D.; Wang, Y.; Li, S.; Jiang, Y.; Jin, M. Effect of lens focusing distance on AlO molecular emission from femtosecond laser-induced aluminum plasma in air. *Opt. Laser Technol.* **2020**, *122*, 105862. [CrossRef]
38. Harilal, S.S.; Yeak, J.; Brumfield, B.E.; Suter, J.D.; Phillips, M.C. Dynamics of molecular emission features from nanosecond, femtosecond laser and filament ablation plasmas. *J. Anal. At. Spectrom.* **2016**, *31*, 1192–1197. [CrossRef]
39. Guo, L.-B.; Hao, R.-F.; Hao, Z.-Q.; Li, K.-H.; Shen, M.; Ren, Z.; Li, X.-Y.; Zeng, X.-Y. Study on the emission spectrum of AlO radical B2+X2+ transition using laser-induced breakdown spectroscopy. *Acta Phys. Sin.* **2013**, *62*, 224211. [CrossRef]
40. Chen, Y.; Dong, M.; Cai, J.; Chen, H.; Shang, Z.; Lu, J. An image auxiliary method for laser-induced breakdown spectroscopy analysis of coal particle flow. *J. Anal. At. Spectrom.* **2022**, *37*, 1126–1133. [CrossRef]
41. Han, W.; Wang, Y.; Yin, Y.; Li, X.; Sun, D.; Su, M. Analysis of metal elements contained in graphite target coated with Chinese medicinal material nanoparticles using LIBS. *Front. Phys.* **2022**, *10*, 862578. [CrossRef]

42. Legnaioli, S.; Campanella, B.; Poggialini, F.; Pagnotta, S.; Harith, M.A.; Abdel-Salam, Z.A.; Palleschi, V. Industrial applications of laser-induced breakdown spectroscopy: A review. *Anal. Methods* **2020**, *12*, 1014–1029. [CrossRef]
43. Tognoni, E.; Cristoforetti, G. [INVITED] Signal and noise in Laser Induced Breakdown Spectroscopy: An introductory review. *Opt. Laser Technol.* **2016**, *79*, 164–172. [CrossRef]
44. Zheng, P.; Chen, G.; Gu, W.; Wang, J.; Hou, Z.; Gao, X.; Chen, A.; Zhou, W.; Guo, L.; Zeng, Q.; et al. Upgrade from signal enhancement to plasma modulation for LIBS signal improvement. *TrAC Trends Anal. Chem.* **2026**, *197*, 118709. [CrossRef]
45. Zhao, S.; Song, C.; Gao, X.; Lin, J. Quantitative analysis of Pb in soil by femtosecond-nanosecond double-pulse laser-induced breakdown spectroscopy. *Results Phys.* **2019**, *15*, 102736. [CrossRef]
46. Yang, X.; Hao, Z.; Yi, R.; Li, J.; Yu, H.; Guo, L.; Li, X.; Zeng, X.; Lu, Y. Simultaneous determination of La, Ce, Pr, and Nd elements in aqueous solution using surface-enhanced laser-induced breakdown spectroscopy. *Talanta* **2017**, *163*, 127–131. [CrossRef]
47. Sládková, L.; Prochazka, D.; Pořízka, P.; Škarková, P.; Remešová, M.; Hrdlička, A.; Novotný, K.; Čelko, L.; Kaiser, J. Improvement of the laser-induced breakdown spectroscopy method sensitivity by the usage of combination of Ag-nanoparticles and vacuum conditions. *Spectrochim. Acta Part B At. Spectrosc.* **2017**, *127*, 48–55. [CrossRef]
48. Cremers, D.A.; Radziemski, L.J. *Handbook of Laser-Induced Breakdown Spectroscopy*; Wiley: Hoboken, NJ, USA, 2006.
49. Tsai, S.J.; Chen, S.Y.; Chung, Y.S.; Tseng, P.C. Spatially resolved, laser-induced breakdown spectroscopy, development, and application for the analysis of Al and Si in nickel-based alloys. *Anal. Chem.* **2006**, *78*, 7432–7439. [CrossRef]
50. Penczak, J.; Liu, Y.; Gordon, R. Polarization Resolved Laser-Induced Breakdown Spectroscopy of Al. *J. Phys. Chem. A* **2009**, *113*, 13310–13317. [CrossRef] [PubMed]
51. Zhao, S.; Zhao, Y.; Hou, Z.; Wang, Z. Stability and accuracy improvement of element analysis in steel alloys using polarization-resolved laser-induced breakdown spectroscopy. *Spectrochim. Acta Part B At. Spectrosc.* **2023**, *203*, 106666. [CrossRef]
52. Eslami Majd, A.; Arabanian, A.S.; Massudi, R. Polarization resolved laser induced breakdown spectroscopy by single shot nanosecond pulsed Nd:YAG laser. *Opt. Lasers Eng.* **2010**, *48*, 750–753. [CrossRef]
53. Lengsfield, B.H., III; Liu, B. Ab initio dipole moment functions for the X 2Σ+ and B 2Σ+ states of AlO. *J. Chem. Phys.* **1982**, *77*, 6083–6089. [CrossRef]
54. Geethika, B.; Thomas, J.; Dave, J.; Joshi, H.C. Effect of polarization on spectroscopic characterization of laser produced aluminium plasma. *Spectrochim. Acta Part B At. Spectrosc.* **2024**, *221*, 107033. [CrossRef]
55. Penczak, J.S., Jr.; Liu, Y.; Schaller, R.D.; Rich, D.H.; Gordon, R.J. The mechanism for continuum polarization in laser induced breakdown spectroscopy of Si (111). *Spectrochim. Acta Part B At. Spectrosc.* **2012**, *74*, 3–10. [CrossRef]
56. Chen, Y.; Liu, Y.; Wang, Q.; Li, S.; Jiang, Y.; Chen, A.; Jin, M. Effect of laser polarization on molecular emission from femtosecond LIBS. *J. Anal. At. Spectrom.* **2022**, *37*, 82–88. [CrossRef]

Disclaimer/Publisher's Note: The statements, opinions and data contained in all publications are solely those of the individual author(s) and contributor(s) and not of MDPI and/or the editor(s). MDPI and/or the editor(s) disclaim responsibility for any injury to people or property resulting from any ideas, methods, instructions or products referred to in the content.